submitted to Phys.Rev.Lett.

Evidence of strong electron-phonon interaction in superconducting MgB_2 from electron tunneling.

A. I. D'yachenko,* V. Yu. Tarenkov,* A. V. Abal'oshev, and S. J. Lewandowski
Instytut Fizyki Polskiej Akademii Nauk, Al. Lotników 32, 02-668 Warszawa, Poland

We report tunneling measurements of the electron-phonon (e-ph) interaction in superconducting MgB_2 using the MgB_2-I-Nb junctions, where I stands for insulator. The phonon structure in tunneling density of states in MgB_2 clearly indicates strong e-ph coupling for the E_{2g} in-plane boron phonons in a narrow range around 60 meV. The Eliashberg spectral function $\alpha^2(\omega)F(\omega)$ reconstructed from the tunneling data, exhibits significant additional contribution into e-ph interaction from other vibrations such as acoustic (~ 38 meV) and optical (~ 90 meV) bands. Our results are in reasonable agreement with neutron scattering experiments, and also to some data of Raman and infrared spectroscopy.

PACS numbers: 74.25.Kc, 74.50.+r, 74.70.-b

The recent discovery of superconductivity near 40K in MgB_2, stimulated a renewed interest in the pairing mechanism of cuprate superconductors. It is generally believed that understanding superconductivity in the simple binary MgB_2 compound should be much easier than in the high-T_c superconductors. Theoretical *ab initio* calculations show that dominant contribution to Eliashberg function in MgB_2 arises from the Raman-active E_{2g} phonons near the Brillouin zone center at ~ 75 meV [1, 2, 3, 4, 5]. This conclusion is supported by Raman studies [3, 6, 7, 8], which indicate a mode at $\sim 600-620$ cm^{-1} ($74-77$ meV) with a very large width ~ 200 cm^{-1} (25 meV), usually related to anharmonic effects. However, there has been no consensus about the energy and role of the E_{2g} mode, because this mode has not been identified unambiguously by inelastic neutron scattering or in Raman experiments [8, 9, 10, 11, 12].

Tunneling spectroscopy can provide a direct measure of the Eliashberg electron-phonon spectral function $\alpha^2(\omega)F(\omega)$, which can reveal the importance of different phonon modes in the superconductivity of MgB_2. Here $F(\omega)$ is phonon density of states and $\alpha(\omega)$ is an effective electron-phonon coupling function for phonons of energy $\hbar\omega$. Tunneling conductivity $\sigma = dI/dV$ gives direct information about the density of states $N(\omega) \propto \mathrm{Re}\{\omega/[\omega^2 - \Delta(\omega)^2]^{1/2}\}$ related to quasi-particle excitations in the superconductor, where $\Delta(\omega)$ is a complex and energy dependent gap function [15]. $\alpha^2(\omega)F(\omega)$ can be obtained by the inversion of the Eliashberg equations for $\Delta(\omega)$ [16, 17]. The method is based on the determination of $\Delta(\omega)$, therefore it non-sensitive to the presence of non-superconducting impurity phases in MgB_2. The latter can give comparable features in Raman and infrared spectra at energy range typical for the superconducting MgB_2 [10, 14].

We report here high resolution superconducting tunneling spectroscopy measurements of the phonon structure of MgB_2. We used tunnel point-contact junctions

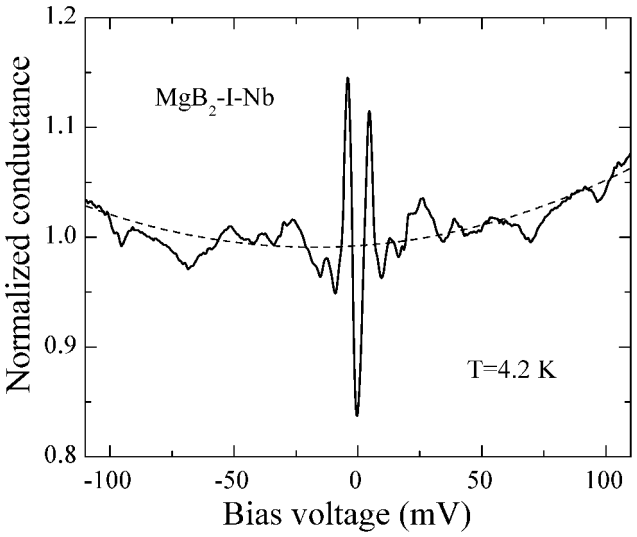

FIG. 1: Experimental conductance of MgB_2-I-Nb tunnel junction in superconducting state (solid line) and the corresponding approximation of the normal state data (dashed line).

Nb-I-MgB_2, where I is a natural tunnel barrier. We found that the second derivative of tunnel current d^2I/dV^2 exhibits features, which coincide with peaks in the phonon density of states (DOS) $F(\omega)$ obtained from neutron scattering [18, 19, 20], Raman [12] and infrared [13, 14] spectroscopy. Numerical treatment of the experimental data indicates that the observed phonon structures between $55-65$ meV and near 90 meV are very strongly coupled to the electrons.

The investigated samples were prepared by compacting commercially available MgB_2 powder (Alfa Aesar, purity 98%) at high pressure ($P > 5$ GPa) into thin rectangular bars of about $1 \times 0.6 \times 0.08$ mm^3. Details of the sample preparation are described elsewhere [21]. The samples revealed a superconductive transition temperature (onset) at $T_c = 38$ K and a high critical cur-

rent density $J_c > 10^5 \mathrm{A/cm^2}$ at T = 4.2 K, considerably larger than the current densities employed in the tunneling measurements. Therefore, current depairing had no effect on the phonon-mediated region of tunneling data. The point-contact junctions were obtained by pressing Nb wire ($\varnothing \sim 50\mu$m) into the surface of the sample. The tunnel characteristics were measured using a standard four probe lock-in technique.

In a number of Andreev S-N-S and tunnel S-I-S experiments at T = 4.2 K we observed two gaps Δ, the smaller gap value of about 3 meV, and a larger gap close to 7 meV, both results in agreement other measurements [22]. In tunnel S-I-S junctions we observed usually only the smaller gap with s-wave symmetry. Let us observe that the smaller ~ 3 meV and the larger ~ 7 meV gaps are associated with the $3d$ parts and quasi-2D sheets of the Fermi surface, respectively [4]. The experimental detection of the single small gap is possible in the case of tunneling perpendicular to the honeycomb born planes. Due to the strong directionality of the tunnelling experiments, the probability of normal injection is maximal and electronic properties are mainly probed along the direction perpendicular to the junction surface, i.e. in our case normal to the born planes.

At high bias voltages (> 20 meV) the $\mathrm{d}I/\mathrm{d}V(V)$ data reveal a structure (Fig.1), which in the case of conventional superconductors is characteristic of phonon effects [23]. To investigate this structure in more detail, we used the second derivative of the tunneling current $\mathrm{d}^2I/\mathrm{d}V^2$, obtained by standard harmonic detection, as well as by straightforward numerical differentiation of the tunneling conductivity $\mathrm{d}I/\mathrm{d}V$. Both methods give analogous results. In these spectra, we observed sometimes peaks at $\sim$ 17 meV and $\sim$ 28 meV, which are not intrinsic to clean MgB_2. The structure near 28 meV most likely arises from a thin pure Mg layer in proximity with the superconducting MgB_2 (analogous structures have been observed in Ag-I-Mg/Nb junctions [24]). For this reason, we excluded these singularities from further considerations, especially as they do not affect the subsequent treatment of the raw data.

The plot $\mathrm{d}^2I/\mathrm{d}V^2(V)$, shown in Fig. 2, at eV > 30 meV directly reflects the electron-phonon spectral function $\alpha^2(\omega)\mathrm{F}(\omega)$ of MgB_2; in particular the dips in $\mathrm{d}^2I/\mathrm{d}V^2$ correspond to peaks in $\alpha^2(\omega)\mathrm{F}(\omega)$. Peaks in $\mathrm{F}(\omega)$ should be reproduced in $\alpha^2(\omega)\mathrm{F}(\omega)$ at approximately the same energy, even if the coupling factor $\alpha^2(\omega)$ is strongly energy dependent. The $\mathrm{d}I/\mathrm{d}V$ and $\mathrm{d}^2I/\mathrm{d}V^2$ data were used to obtain the normalized tunneling conductance σ/σ_N, where σ_N is a normal-state (background) conductance, and the tunneling density of states $N(\omega)$; the relevant numerical method is given in [23].

The normalized density of states $n(\omega) = N(\omega)/N_{\mathrm{BCS}}(\omega) - 1$, proportional to the smoothed $\mathrm{d}I/\mathrm{d}V$ curve, is shown in Fig. 3. Here $N_{\mathrm{BCS}}(\omega)$ is the broadened BCS density of states (Dynes function).

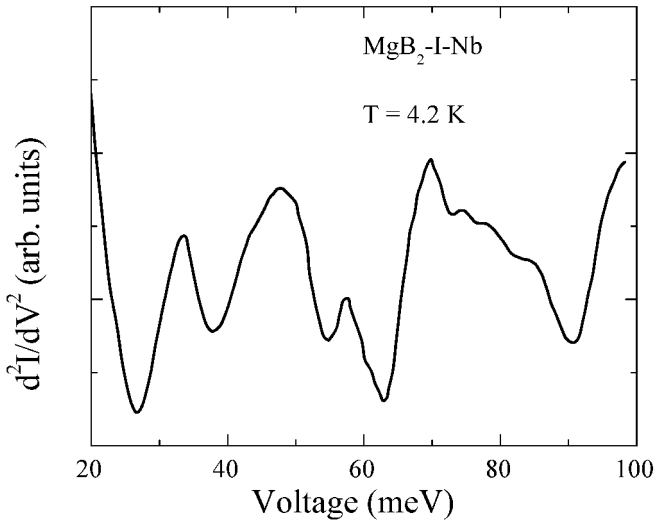

FIG. 2: Second derivative $\mathrm{d}^2I/\mathrm{d}V^2$ plots of a MgB_2-I-Nb junction. The minima in the curve correspond to peaks in Eliashberg function $\alpha^2(\omega)\mathrm{F}(\omega)$. Voltage origin is at $\Delta_{MgB_2} + \Delta_{Nb}$

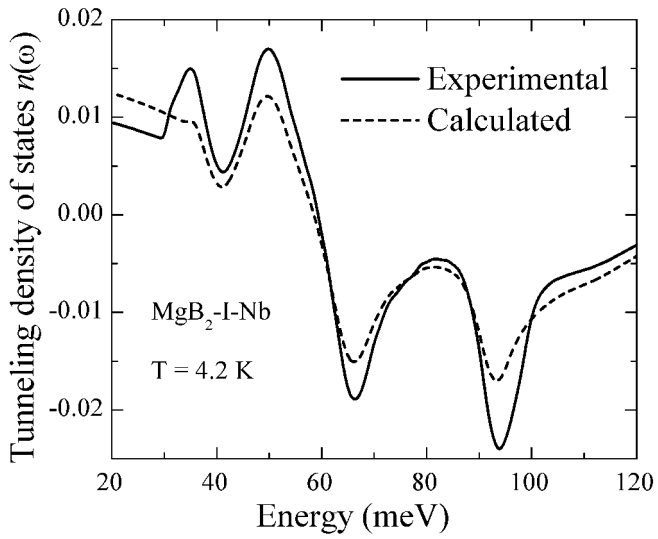

FIG. 3: The tunneling density of states of MgB_2 $n(\omega)$, normalized to the BCS density of states. Experimental data are plotted as a solid line; dashed line shows $n(\omega)$ calculated from Eliashberg function $\alpha^2(\omega)\mathrm{F}(\omega)$.

The $\mathrm{d}I/\mathrm{d}V$ curve displays a well-known behavior due to the phonon mode reflection in tunneling S-I-S conductance [15, 16], namely, sharp drops of $\mathrm{d}I/\mathrm{d}V$ near the phonon emission thresholds, to which correspond dips in $\mathrm{d}^2I/\mathrm{d}V^2$. We can rule out very weak inelastic process of phonon-assisted tunneling, because such process increases the tunneling conductance near the peaks in $\mathrm{F}(\omega)$ and gives corresponding peaks in $\mathrm{d}^2I/\mathrm{d}V^2$ [23]. The common feature of all measured $\mathrm{d}^2I/\mathrm{d}V^2$ curves is the reproducibility of dip positions at $\sim$ 40, $55 \div 65$ and $90 \div 92$ meV, measured from the gap sum

$\Delta_{MgB_2} + \Delta_{Nb}$ (Fig.2). There is a close correlation in the peak positions in our d^2I/dV^2 data and thouse in the generalized phonon density of states (GPDOS) as measured by inelastic neutron scattering data [18, 19]. The first tunneling peak near 40 meV arises from acoustic modes of MgB_2. The well-resolved tunneling structures at $\sim$ 60 meV and $\sim$ 90 meV are associated with optical vibration of the born atoms. As it is well known, in the vicinity of peaks in $\alpha^2(\omega)F(\omega)$, the gap function $\Delta(\omega)$ has a strong energy dependence and large $\mathrm{Im}\{\Delta(\omega)\}$ [15]. At $\hbar\omega \gg |\Delta|$ tunneling density $N(\omega) \sim 1 + (1/2)\mathrm{Re}\{\Delta^2(\omega)/\omega^2\}$, so the phonon structure in $N(\omega)$ is weighted by the factor $(\delta\Delta/\omega)^2$. In the strong coupling limit (the McMillan's electron-phonon coupling constant λ of the order of 1) variation of $\Delta(\omega)$, $\delta\Delta \sim \Delta$, and the deviation in $N(\omega)$ is of the order $1-2\%$ (Fig.3). Even without detailed calculations one can see that since the amplitude of tunneling structure at 40 meV is roughly one half of that at 60 meV (c.f. Fig.2) and the optical phonon energy is 1.5 times higher, the actual electronic coupling to the phonons at 60 meV may be as much as $(1.5)^2 \sim 3$ times greater than that for acoustic phonons at $\sim$ 40 meV. On the other hand, it is evident, that the optical modes at $\sim$ 90 meV give approximately the same contribution than that of modes at 60 meV. Such conclusion, obtained directly from the tunneling data, is independent of the anisotropy of the energy gap $\Delta(\mathbf{k})$ and agrees well with similar estimations based upon Raman and infrared spectra measurements [13, 14].

An exact determination of $\alpha^2(\omega)F(\omega)$ requires full inversion of the Eliashberg equations. We used normalized conductivity σ/σ_N for self-consistent calculation of the spectral function $\alpha^2(\omega)F(\omega)$ with a standard inversion program [23], which allows to take into account the already mentioned possible presence of a thin Mg layer on the surface of MgB_2, in which reduced superconductivity is induced by proximity effect. The gap edge region below 26 meV was cut off to avoid a divergence of DOS. The obtained "experimental" function $\alpha^2(\omega)F(\omega)$ is shown in Fig.4 together with theoretical *ab initio* phonon density of states $F_t(\omega)$ combined with neutron scattering [19]. In isotropic limit for $\lambda = 0.9$ and $\mu^* = 0.1$ Eliashberg function yields $T_c \approx 38$ K, and $|\Delta| = 6.5$ meV. Neutron GPDOS [18, 19] differs in its detailed shape from $F_t(\omega)$, but peaks in $F_t(\omega)$, GPDOS and our $\alpha^2(\omega)F(\omega)$ all occur at the same energies. They all show pronounced minima at $40 \div 50$ meV and maxima at 37, 62 and $90 \div 92$ meV. The peak in $\alpha^2(\omega)F(\omega)$, responsible for acoustic bands ($\sim$ 38 meV), is strongly suppressed, but does not disappear completely, as in the theoretical calculations [1, 4]. We do not see also the prevailing amplitude of one mode at $60-70$ meV, as predicted for the theoretical function $\alpha^2(\omega)F_t(\omega)$ [1, 4, 5], although our experimental data indicate two bands of optical modes corresponding primarily to the born motions at $\sim$ 60 and $\sim$ 90 meV. For comparison, in Fig.4(b) the calculated phonon dispersion curves are shown along the high-symmetry directions of the Brillouin zone [19]. As seen, the E_{1u} and A_{2u} infrared active modes give noticeable contribution to the $\alpha^2(\omega)F(\omega)$ at 40 and 50 meV, respectively. They have been also observed in infrared absorption experiments at 333 cm^{-1} (41 meV) and 387 cm^{-1} (48 meV)[14]. Optical studies in the c-axis oriented superconducting MgB_2 films show two strong phonon peaks at 380 cm^{-1} (48 meV) and 480 cm^{-1} (60 meV) [13]. The peak in the "experimental" $\alpha^2(\omega)F(\omega)$ at $60 \div 65$ meV arises mainly from the E_{2g} phonon modes with wave vector along the $\Gamma-A$ direction [Fig.4(b)]. This phonon mode is Raman-active. In most investigations the Raman scattering in MgB_2 revealed a broad peak near 620 cm^{-1} (78 meV) but, Meletov *et al*

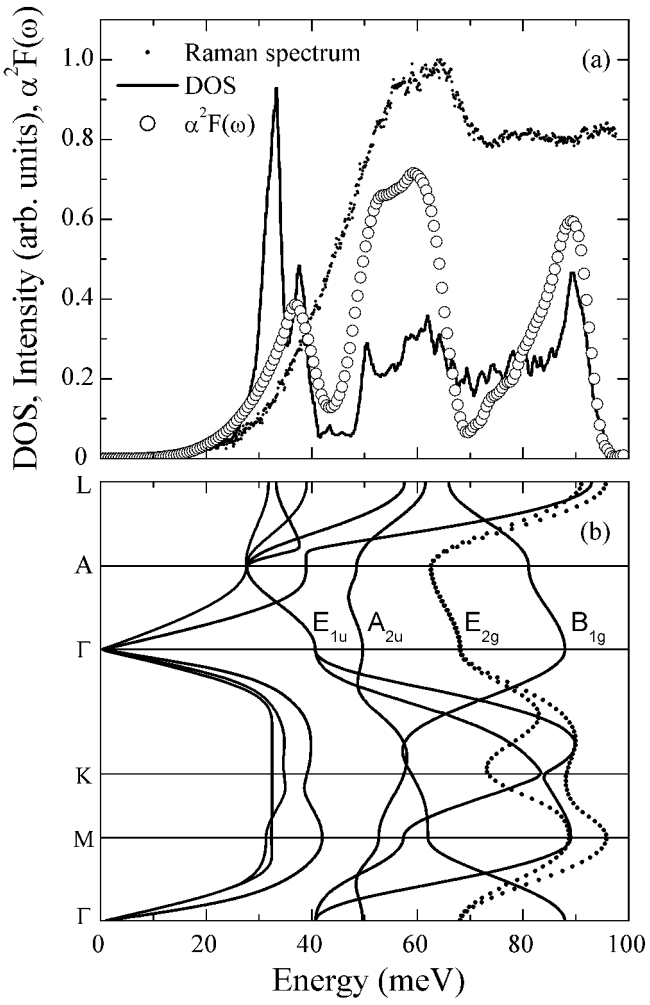

FIG. 4: Comparison of the phonon density of states in MgB_2 obtained by different methods. (a) The function $\alpha^2(\omega)F(\omega)$ of MgB_2, determined from tunneling measurements in this work (open circles). The continues curve is the phonon density of states $F_t(\omega)$ calculated from neutron data [19]. The dotted curve shows Raman spectra of MgB_2 at room temperature [12], for the sample obtained under high pressure. (b) The calculated phonon dispersion curves [19].

[12] have observed a peak near ~ 590 cm^{-1} (73 meV). They investigated ceramic MgB_2 samples using a micro-Raman system, which rendered possible the identification of small crystalline grains of MgB_2, whose Raman spectra differ drastically from those of MgO or metallic Mg inclusions. After homogenisation of ceramic samples induced by high pressure (> 5 GPa) the E_{2g} phonon mode was observed at $500 - 550$ cm^{-1} ($62 - 68$ meV) [the dotted curve at Fig. 4(a)], which is close to our $\alpha^2(\omega)F(\omega)$ result. For the E_{2g} mode, there are also large discrepancies between the results of various calculations. For example, the harmonic energy $\omega_H(E_{2g}) = 60$ meV [19], but anharmonicity leads to an increase of $\omega_H(E_{2g})$ up to 75 meV [1, 19]. Approximately the latter value (75 meV) was reported in the Raman study [7], where E_{2g} mode had very large (~ 25 meV) width. On the other hand, our experimental $\alpha^2(\omega)F(\omega)$ coincides best with the harmonic value $\omega_H(E_{2g}) \sim 60$ meV [19] (Fig.4) and is reasonably narrow. The extremely broad E_{2g} line at ~ 620 cm^{-1} (78 meV) can include a sum of peaks from impurity phases, like Mg, MgO (phonon mode of MgO at ~ 80 meV has been observed in Ref. [25]), B_2O_3, and second-order Raman signal from the acoustic ~ 300 cm^{-1} (37 meV) phonon [10]. On the other hand, the infrared absorption spectrum of MgB_2 is characterized by a broad band centered at 485 cm^{-1} (60 meV) [14], which can be associated with the peak in phonon density of states $F(\omega)$ at 60 meV, in agreement with our results (Fig.4).

In summary, we have obtained high resolution tunneling spectra of MgB_2 with $T_c = 38$ K. The tunneling density of states deviated from the standard Dynes function above 30 meV in a way, which is characteristic of phonon effects. The second derivative curve displays dips at energies, which correspond to peaks in the phonon density of states measured by neutron scattering an also to some data of Raman and infrared spectroscopy. The spectral function $\alpha^2(\omega)F(\omega)$ has been reconstructed from tunneling data. The relatively big structure in tunneling spectra confirms strong coupling of electrons to optical E_{2g} phonon modes at ~ 60 meV. However, other vibrations such as acoustic (~ 38 meV) and optical (~ 90 meV) bands are also important and give noticeable peaks in the tunneling spectra. Therefore, the predominance of the E_{2g} phonon mode near the Γ point in the electron-phonon mechanism of superconductivity in MgB_2 may be questioned.

This work was supported by Polish Government (KBN) Grant No PBZ-KBN-013/T08/19.

* permanent address: Donetsk Physico-Technical Institute, Ukrainian National Academy of Sciences, R.Luxemburg St. 72, 340114 Donetsk, Ukraine.

[1] Y. Kong, O.V. Dolgov, O. Jepsen, and O.K. Andersen, Phys. Rev. B **64**, 20501 (2001).
[2] J.M. An and W.E. Pickett, Phys. Rev. Lett. **86**, 4366 (2001).
[3] K.-P. Bohnen, R. Heid, and B. Renker, Phys. Rev. Lett. **86**, 5771 (2001).
[4] Amy Y. Liu, I.I. Mazin, and Jens Kortus, Phys. Rev. Lett. **87**, 087005 (2001).
[5] J. Kortus, I.I. Mazin, K.D. Belashchenko, V.P. Antropov, and L.L. Boyer, Phys. Rev. Lett. **86**, 4656 (2001).
[6] A.F. Goncharov, V.V. Struzhkin, E. Gregoryanz, Jingzhu Hu, R.J. Hemley, Ho-kwang Mao, G. Lapertot, S.L. Bud'ko, and P.C. Canfield, Phys. Rev. B **64**, 100509 (2001).
[7] J. Hlinka, I. Gregora, J. Pokorný, A. Plecenik, P. Kúš, L. Satrapinsky, Š. Beňačka, Phys. Rev. B **64**, 140503 (2001).
[8] K. Kunc, I. Loa, K. Syassen, R.K. Kremer, K. Ahn, cond-mat/0105402.
[9] X.K. Chen, M.J. Konstantinović, J.C. Irwin, D.D. Lawrie, and J.P. Franck, Phys. Rev. Lett. **87**, 157002 (2001).
[10] P.M. Rafailov, S. Bahr, and C. Thomsen, Phys. Stat. Solodi B **226**, R9 (2001).
[11] V.V. Struzhkin, A.F. Goncharov, R.J. Hemley, H.K. Mao, G. Lapertot, S.L. Bud'ko, and P.C. Canfield, cond-mat/0106576.
[12] K.P. Meletov, J. Arvanitidis, M.P. Kulakov, N.N. Kolesnikov, and G.A. Kouroukis, cond-mat/0110511.
[13] J.J. Tu, G.L. Carr, V. Perebeinos, C.C. Homes, M. Strongin, P.B. Allen, W.N. Kang, E.M. Choi, H.J. Kim, and Sung-Ik Lee, Phys. Rev. Lett. **87**, 277001 (2001).
[14] C.S. Sundar, A. Bharathi, M. Premila, T.N. Sairam, S. Kalavathi, G.L.N. Reddy, V.S. Sastry, Y. Hariharan, and T.S. Radhakrishnan, cond-mat/0104354.
[15] J.R. Schrieffer, D.J. Scalapino, and J.W. Wilkins, Phys. Rev. Lett. **10**, 336 (1963).
[16] W.L. McMillan and J.M. Rowell, Phys. Rev. Lett. **14**, 108 (1965).
[17] A.A. Galkin, A.I. D'yachenko, and V.M. Svistunov, Sov. Phys. JETP **39**, 1115 (1974).
[18] R. Osborn, E.A. Goremychkin, A.I. Kolesnikov, and D.G. Hinks, Phys. Rev. Lett. **87**, 017005 (2001).
[19] T. Yildirim, O. Gülseren, J.W. Lynn, C.M. Brown, T.J. Udovic, Q. Huang, N. Rogado, K.A. Regan, M.A. Hayward, J.S. Slusky, T. He, M.K. Haas, P. Khalifah, K. Inumaru, and R.J. Cava, Phys. Rev. Lett. **87**, 037001 (2001).
[20] E.S. Clementyev, K. Conder, A. Furrer, and I.L. Sashin, Eur. Phys. J. B **21**, 465 (2001).
[21] A.I. D'yachenko, V.Yu. Tarenkov, R. Szymczak, A.V. Abal'oshev, I.S. Abal'osheva, S.J. Lewandowski, and L. Leonyuk, Phys. Rev. B **61**, 1500 (2000).
[22] C. Buzea and T.Yamashita, Supercond. Sci. Technol. **14**, R115 (2001).
[23] E. L. Wolf, *Principles of Electron Tunneling Spectroscopy* (Oxford University Press, New York, 1985).
[24] D.M. Burnell and E.L. Wolf, Phys. Lett. A **90**, 471 (1982).
[25] J.G. Adler, Solid State Commun. **7**, 1635 (1969).